

Initial Conditions Contribution in Frequency-Domain BEM Analysis

W. J. Mansur¹, A. I. Abreu¹ and J. A. M. Carrer¹

Abstract: This work is concerned with the computation of the contribution of initial conditions in two-dimensional (2D) frequency-domain analysis of transient scalar wave propagation problems with the corresponding Boundary Element Method (BEM) formulation. The paper describes how pseudo-forces, represented by generalized functions, can replace the initial conditions, related to the potential and its time derivative. The generation of such pseudo-forces is the subject of a detailed discussion. The formulation presented here carries out Discrete Fourier Transform (Direct: DFT, and Inverse: IDFT) via FFT (Fast Fourier Transform) algorithms. At the end of the paper four examples are presented in order to show the potentialities and accuracy of the approach.

keyword: Boundary elements, Helmholtz equation, frequency domain, scalar wave equation, Fourier transform, initial conditions.

1 Introduction

Several BEM formulations have been developed so far in order to solve problems governed by the scalar wave equation. For general purposes, time-domain (TD) and transformed-domain formulations can be employed to solve scalar wave propagation problems. Time-domain BEM formulations (TD-BEM), e.g., Mansur (1983), Dominguez (1993), Antes and Von Estorff (1987), Mansur, Carrer and Siqueira (1998), provide good representation of causality and time response jumps and lead to accurate results. Besides, the fulfillment of the radiation condition makes them suitable for infinite domain analysis. The computational cost, however, is high when late time results are required due to the convolution performed from the initial time to the current time. To avoid such a high computational cost without a significant loss of accuracy, truncation techniques, such as that presented

by Mansur and DeLima-Silva (1992) can be employed.

Transformed-domain BEM formulations also have been the subject of intense research work and are mainly related either to the frequency-domain approach, e.g., Dominguez (1993), Godinho, Tadeu and Branco (2003), Gaul and Wenzel (2002), or to the Laplace-domain approach, e.g., Cruse and Rizzo (1968), Manolis and Beskos (1981), etc. When employing these formulations, the problem is initially solved in the transformed-domain for a suitable number of discrete values of the transform parameter and, when required, the solution in the time-domain can be obtained by means of a suitable inverse transformation procedure, e.g., Dubner and Abate (1983) and Durbin (1974) for Laplace transform, and the well known DFT (or FFT) algorithms for Fourier transform. It is worth mentioning that some very attractive meshless approaches to do frequency-domain modeling with BEM have been subject of intensive research in recent years, e.g., the MLPG (LBIE) method presented by Sellountos and Polyzos (2003).

A very promising approach which has been more and more employed is that based on the Operational Quadrature Method (Lubich (1988), Gaul and Schanz (1999)) recently applied to crack analysis by Zhang and Savaidis (2003).

Besides the aforementioned formulations, it is important to mention alternative TD-BEM approaches that employ “static” fundamental solutions related to the problem analysed: in the case of time-domain analysis, two BEM formulations that employ the static fundamental solution have been employed successfully so far. According to the treatment given to the domain integrals concerning inertial terms one has: the so-called D-BEM (D meaning domain), that maintains the domain integrals, e.g., Carrer and Telles (1992) and Hatzigeorgiou and Beskos (2001), and the DR-BEM (DR meaning dual-reciprocity). The latter transforms domain integrals into boundary integrals, by means of suitable interpolation functions as described by Nardini and Brebbia (1985)

¹ Department of Civil Engineering,
COPPE / Federal University of Rio de Janeiro
CXP 68506, CEP: 21945-970, Rio de Janeiro, RJ, Brasil
e-mail address; webe@coc.ufrj.br (W. J. Mansur)

and Partridge, Brebbia and Wrobel (1992). The common feature between them is that it becomes possible to use step-by-step time-marching procedures, similar to those employed in the Finite Element formulation.

This work presents a BEM frequency-domain formulation that takes into account initial conditions contribution in the solution of problems governed by the scalar wave equation. Unlike Laplace-domain formulations, in which initial conditions appear explicitly in the transformed-domain equilibrium equations, authors who deal with frequency-domain formulations do not consider non-null initial conditions, e.g., Clough and Penzien (1993). In this article, this difficulty was overcome in a very elegant and simple way; basically, the methodology used consists of replacing the initial conditions (related to the potential and its time derivative) by pseudo-forces, represented by generalized functions. In the appropriate section of this work, a detailed discussion concerning the various aspects of this methodology denoted here ICPF (Initial Conditions by Pseudo-Forces) is carried out.

Linear boundary elements and linear triangular cells have been employed in the BEM formulation. The reader is referred to Mansur (1983) and Carrer and Mansur (1996) for general aspects concerning boundary and domain integration.

At the end of the paper, four examples are presented to validate the formulation and verify its accuracy and robustness.

2 Boundary Element for the Helmholtz equation

The starting BEM equation corresponding to Helmholtz equation in $\Omega \cup \Gamma$, for 2D problems, can be written as Dominguez (1993):

$$\begin{aligned} c(\xi)U(\xi) &= \int_{\Gamma} U(X)p^*(X,\xi)d\Gamma - \int_{\Gamma} P(X)u^*(X,\xi)d\Gamma \\ &+ \int_{\Omega} B(X)u^*(X,\xi)d\Omega \end{aligned} \quad (1)$$

where $B(X)$ is a Ω domain body force, $X = X(x, y)$ indicates spatial dependency and the Γ boundary is assumed to be constituted by $\Gamma = \Gamma_u \cup \Gamma_p$, Neumann and Dirichlet boundary conditions being respectively prescribed on Γ_u and Γ_p . In eq. (1), one has $c(\xi) = 1$ when $\xi \in \Omega$ and $c(\xi) = \alpha/2\pi$ when $\xi \in \Gamma$ (α is the internal angle formed by tangents to Γ at ξ). In the above expression, $u^*(X, \xi)$

is the fundamental solution and $p^*(X, \xi) = \partial u^*(X, \xi)/\partial \mathbf{n}$. Their expressions are given by (Morse and Feshbach (1953):

$$\begin{aligned} u^*(r, \gamma) &= \frac{-i}{4} H_0^{(1)}(\gamma r) \\ p^*(r, \gamma) &= \frac{i\gamma}{4} H_1^{(1)}(\gamma r) \frac{\partial r}{\partial \mathbf{n}} \end{aligned} \quad (2)$$

where γ is the wave number computed according to: $\gamma = \omega/c$, ω being the circular frequency and c the wave propagation velocity, $r = |X - \xi|$ is the Euclidian distance between field X and source ξ points, $H_0^{(1)}$ and $H_1^{(1)}$ are the Hankel functions of first type and zero and first order, respectively (note that the wave number was not shown as argument in expression (1)).

The application of the discretized version of eq. (1) to all boundary nodes produces a system of algebraic equations, represented as follows:

$$\mathbf{H} \mathbf{U} = \mathbf{G} \mathbf{P} + \mathbf{B} \quad (3)$$

Taking into account the boundary conditions, the system of equations (3) can be written according to:

$$\mathbf{A} \mathbf{X} = \mathbf{Y} + \mathbf{B} \quad (4)$$

After solving the system of equations (4), all the boundary variables (potential and flux) are known and the potential at internal points ξ ($\xi \in \Omega$) can be computed from eq. (1) if one takes $c(\xi) = 1$.

Therefore eq. (4) is a discrete integral form which produces approximate solutions of Helmholtz equation subjected to boundary conditions.

3 Frequency-domain analysis

Frequency-domain analysis using standard Discrete Fourier Transform (DFT) or Fast Fourier Transform (FFT) algorithms (Clough and Penzien (1993), Oppenheim and Schaffer (1989), Paz (1997) and Brigham (1974)) can only be carried out if damping (viscous, hysterical, geometrical, etc.) exists, due to the singularities in the frequency spectrum at the natural frequencies, and also because undamped systems responses do not follow the theoretical decay condition as $t \rightarrow \infty$, which renders Fourier transform possible. It is important to notice that extending the period, as required when DFT/FFT algorithms are employed, can be unnecessary when the procedure described by Veletsos and Ventura (1984,1985)

can be applied. According to Morse and Feshbach (1993) (see also Chin (1994) and Graff (1975)), in the presence of damping, the wave equation can be written as:

$$c^2 \nabla^2 u(X, t) - c_v \frac{\partial u(X, t)}{\partial t} - \frac{\partial^2 u(X, t)}{\partial t^2} = b(X, t) \quad (5)$$

where c is the wave propagation velocity, and c_v is a coefficient related to coefficient of viscous damping b_v ($c_v = b_v/\rho$). A particular solution to equation (5) can be obtained as long as boundary and initial conditions given respectively by equations (6) and (7) are known (more general boundary conditions are also possible but have not been considered here).

$$u(X, t) = \bar{u}(X, t) (X \in \Gamma_u);$$

$$\frac{\partial u(X, t)}{\partial \mathbf{n}} = \bar{p}(X, t) (X \in \Gamma_p) \quad (6)$$

$$u(X, 0) = u_o(X);$$

$$v(X, 0) = \left. \frac{\partial u(X, t)}{\partial t} \right|_{t=0} = v_o(X) \quad (7)$$

Applying the Fourier transform to eq. (5), a *generalized Helmholtz equation* is obtained:

$$\nabla^2 U(X) + \gamma_c^2 U(X) = B(X) \quad (8)$$

where the wavenumber γ_c is a complex variable, given by:

$$\gamma = \left(\frac{\omega^2}{c^2} - i\omega \frac{c_v}{c^2} \right)^{1/2} \quad (9)$$

The Fourier transforms of $u(X, t)$ and $b(X, t)$ are represented, respectively, by the complex quantities $U(X) = U(X, \omega)$ and $B(X) = B(X, \omega)$. After applying the Fourier transform to the boundary conditions given by eq. (6), the same steps presented in the previous section must be followed in order to obtain equation (4), which now will correspond to a frequency of the Fourier spectrum: one must note that the fundamental solution, in this case, is a function of the complex wavenumber γ_c .

3.1 Numerical procedure

The numerical model employed considers the Γ boundary discretized by linear elements whereas the part of

the Ω domain, where non-homogeneous initial conditions appear, say Ω_0 , is discretized by linear triangular cells.

Once the spectrum of $b(X, t)$, $B(X, \omega_{nt})$ and that of the prescribed boundary conditions have been obtained, NT harmonic problems governed by equation (8) have to be solved ($nt = 1, \dots, NT$; where NT is the total number of frequencies). The responses at boundary nodes and internal points can be stored in matrix form (named, frequency depend matrix $\mathbf{M}(\omega)$ for instance) and the final time-dependent responses (named, \mathbf{u}_b for instance) are computed by applying the Inverse Discrete Fourier Transform (IDFT) to $\mathbf{M}(\omega)$.

When one employs DFT (or FFT) algorithms it is necessary to make a good guess of the extended period "length". Good results have been reported in the literature, e.g., Mansur, Ferreira, Claret, Venâncio-Filho and Carrer (2000), when the period extension is such that the "amplitude" decays, at the end of the period, to 1% of its initial value. As the highest contribution for the displacement is due fundamentally to the first vibration mode, and considering an exponential time decay, one can write:

$$e^{\zeta \omega_1 T_p} = \frac{1}{100} \Rightarrow T_p = \frac{\ln(100)}{\zeta \omega_1} \quad (10)$$

In the above expression ζ is the damping ratio related to the first vibration mode, ω_1 is the fundamental eigenfrequency and T_p is the *extended period*. It is important to recall that the maximum frequency spectrum frequency (*Nyquist frequency*) is $\omega_{max} = \pi/\Delta t$, thus if the problem response contains relevant contributions for $\omega_{nt} > \omega_{max}$, the time response will not be accurate due to aliasing (Oppenheim and Schaffer (1989), Paz (1997) and Brigham (1974)). It is important to mention that although expression (10) tends to overestimate the extended period, it is still a good initial guess, an optimum choice, though, may depend strongly on the experience one has with frequency-domain approaches.

4 Initial Conditions Contribution

Due to the linearity of the problem, the initial conditions and other contributions can be studied separately and the corresponding solutions can be added together to obtain to the final response. Although the methodology is quite general, its basic steps will be presented and discussed for the 2D case.

4.1 Initial displacement

The response corresponding to an initial displacement field $u_o(X)$ is computed by adding to the initial displacement field itself the response corresponding to a suddenly applied load $-f_{u_o}(X)H(t-0)$ ($H(t-0)$ is the Heaviside function). This load $-f_{u_o}(X)$ is a reactive static domain force obtained from eq. (1) when it is particularized to the Poisson equation, i.e., when $\gamma = 0$ and the corresponding Green's function is employed rather than that indicated by eq. (2). Replacing $B(X)$ by $f_{u_o}(X)$ in eq. (1), one can write:

$$\Phi \begin{bmatrix} \mathbf{f}_{u_o}^b \\ \mathbf{f}_{u_o}^d \end{bmatrix} = \left(\begin{bmatrix} \mathbf{H}^{bb} & \mathbf{O} \\ \mathbf{H}^{db} & \mathbf{I} \end{bmatrix} \begin{bmatrix} \mathbf{u}_o^b \\ \mathbf{u}_o^d \end{bmatrix} - \begin{bmatrix} \mathbf{G}^{bb} \\ \mathbf{G}^{db} \end{bmatrix} \begin{bmatrix} \mathbf{p}_o^b \end{bmatrix} \right) \quad (11)$$

or, in a compact notation:

$$\Phi \mathbf{f}_{u_o} = [\mathbf{H}\mathbf{u}_o - \mathbf{G}\mathbf{p}_o] \quad (12)$$

Note that \mathbf{f}_{u_o} is the static reactive force vector which results from a prescribed static field \mathbf{u}_o .

In expressions (11) and (12), Φ is the matrix resulting from the domain integration. As mentioned in the introduction of this work, the domain integration is restricted to the part of the domain with non-homogeneous initial conditions. Additionally, matrices \mathbf{H} and \mathbf{G} are assembled in a unified way to take into account the contribution of the initial displacements in the computation of boundary $\mathbf{f}_{u_o}^b$ and domain $\mathbf{f}_{u_o}^d$ unknowns. The distinction between the positions occupied by source and field points is done by the superscripts b and d : b means boundary and d means domain. Matrices \mathbf{H}^{bb} and \mathbf{G}^{bb} are related to the boundary integral equation; matrices \mathbf{H}^{bd} and \mathbf{G}^{bd} , on the other hand, are obtained when $\xi \in \Omega_o$ and the integration is carried out on the boundary (in other words, they are the matrices related to the integral equation written for internal points). The identity matrix \mathbf{I} appears because for internal point one has (ξ) .

In the assemblage of the matrices \mathbf{H} and \mathbf{G} shown in eq. (12), as $\gamma = 0$, the corresponding expressions for $u^*(X, \xi)$ and $p^*(X, \xi)$ are given by:

$$u^*(r) = \frac{-1}{2\pi} \ln(r)$$

$$p^*(r) = \frac{-1}{2\pi r} \frac{\partial r}{\partial \mathbf{n}} \quad (13)$$

It is important to notice that vectors \mathbf{u}_o and \mathbf{p}_o in eq. (12) are both known. When $grad(u_o(X))$ is discontinuous, in every point i where this discontinuity exists, additional boundary $(\mathbf{p}_o^b)_i$ and/or domain $(\mathbf{p}_o^d)_i$ line force appears. Thus, line forces contributions will have to be considered, through line integrals as shown in the examples of section 5 (a discussion is presented in example 5.4). Line forces distribution will appear when eq. (12) is solved even when not *a priori* considered; however, a very fine mesh is required in order to have a good approximation to such a localized effect. The best representation can be achieved if one is able to identify discontinuities of \mathbf{u}_o space derivatives and thus compute equivalent forces either analytically or numerically. In fact, eq. (12) need not be employed at all to compute \mathbf{f}_{u_o} , it is sufficient to compute the Laplacian of u_o ($c^2 \nabla^2 u_o$) as u_o is known. However, employing eq. (12) may lead to more accurate results than those obtained taking second derivatives of a given $u_o(X)$ function, when analytical expression for $u_o(X)$ is not known.

Due to the periodicity implicit in the Fourier transform approach, the time response produced by the force $\mathbf{f}_{u_o}H(t-0)$ can not be computed correctly, i.e., as DFT algorithms consider periodic functions they do not recognize the jump that occur at the initial time when the applied force is kept constant until the end of the analysis. It is possible to overcome this drawback by assuming the extended period equal to $2T_p$, and by considering \mathbf{f}_{u_o} constant within the time interval $[0, T_p]$ and null within the interval $[T_p, 2T_p]$.

Once the dependence on time of \mathbf{f}_{u_o} is established as explained before, the Fourier transform of \mathbf{f}_{u_o} can be computed and the response spectrum represented by $\mathbf{X}_{u_o}^{nt}$ can be obtained from the solution of the eq. (14) for all the frequencies ($\mathbf{F}_{u_o}^{nt}$ is the frequency spectral vector corresponding to \mathbf{f}_{u_o}):

$$\mathbf{A}\mathbf{X}_{u_o}^{nt} = -\mathbf{F}_{u_o}^{nt} \quad (14)$$

The time-domain response, \mathbf{x}_{u_o} , is computed by applying the IDFT algorithm to the matrix $\mathbf{M}(\omega)$ that stores all the frequency responses at boundary nodes and internal points.

The final response \mathbf{u}_{id} (*id* means initial displacement) due to the initial displacement \mathbf{u}_o is calculated by adding to the initial displacement the response due to $-\mathbf{f}_{u_o}$, i.e.:

$$\mathbf{u}_{id} = \mathbf{x}_{u_o} + \mathbf{u}_o \quad (15)$$

4.2 Initial velocity

The response due to the initial velocity $v_o(X)$ can be computed from the condition “impulse = momentum change”, i.e., the effect of the initial velocity is the same as that of the impulsive force $\rho v_o(X)\delta(t-0)$. The discrete time series $f_{v_o}(X)_r$ of the external force that considers this effect, in what DFT/FFT algorithms are concerned, is defined as follows:

$$f_{v_o}(X)_r = \begin{cases} \frac{\rho v_o(X)}{\Delta t} & \text{for } r = 1 \ (t = 0) \\ 0 & \text{for } r > 1 \end{cases} \quad (16)$$

where ρ is the mass density per unit area and Δt is the time sampling interval. The force $f_{v_o}(X, t)$ should be applied at each nodal point of the domain mesh, and as a domain force, computed according to eq. (8), it must be divided by $E = c^2\rho$ (E is the Young modulus). Thus the vector of nodal impulsive forces which will give the contribution equivalent to the known initial velocity $v_o(X)$ is:

$$(\mathbf{f}_{v_o})_r = \frac{\mathbf{v}_o}{c^2 \Delta t} \delta_{1r} \quad (17)$$

where the vector \mathbf{v}_o in expression (17) is the spatial discretized form of $v_o(X)$ and δ_{1r} is the Kroenecker delta. The Fourier spectrum of \mathbf{f}_{v_o} , denoted by $\mathbf{F}_{v_o}^{nt}$ is then computed, and a procedure similar to that explained previously for the pseudo-force $-\mathbf{f}_{u_o}$ is followed, i.e., the boundary response spectrum due to the initial velocity is computed from:

$$\mathbf{A} \mathbf{X}_{v_o}^{nt} = \mathbf{F}_{v_o}^{nt} \quad (18)$$

The responses in the frequency-domain at the internal points are computed and the NT time dependent responses \mathbf{x}_{v_o} are computed using the IDFT algorithm. Finally, the response for the initial displacement and velocity contributions is given by (ic means initial conditions):

$$\mathbf{u}_{ic} = \mathbf{u}_{id} + \mathbf{x}_{v_o} \quad (19)$$

If the problem presents sources such as $b(X, t)$, the corresponding final response \mathbf{u}_{final} in the time-domain is the sum of all the contributions and is written as:

$$\mathbf{u}_{final} = \mathbf{u} + \mathbf{u}_b + \mathbf{u}_{ic} \quad (20)$$

where \mathbf{u} and \mathbf{u}_b are respectively responses due to boundary conditions and sources.

5 Examples

Four numerical applications are analysed next in order to verify the accuracy of the numerical results provided by the formulation presented in this work. The dimensionless parameter $\beta = c \Delta t / l$, was used to estimate the time-step length (l is the smallest boundary element length).

The FFT and the Inverse Fast Fourier Transform (IFFT) algorithms Brigham (1974) were used with the aim of reducing the computational effort. As defined in section 3.1, the response at boundary nodes and internal points can be stored in a frequency depend matrix $\mathbf{M}(\omega)$. As $\mathbf{M}(\omega)$ and $\mathbf{M}(-\omega)$ are complex conjugate matrices $\mathbf{M}(\omega)$ is calculated only at $NT/2$ points (note that $\mathbf{M}(\omega = 0)$ and $\mathbf{M}(\omega = \omega_{NT/2})$ are real). The 2D responses were compared with the corresponding one-dimensional responses, determined in the same manner using this new methodology (Mansur, Abreu, Carrer and Ferro (2002)).

The following parameters were adopted for the one-dimensional examples (sections 5.1, 5.3 and 5.4): length $L = 12$, $c = 1$ and $\zeta = 0.016$, $2Tp = 1842.3808$ (Tp was estimated by expression (10) taking $\omega_1 = \pi c / 2L$). The one-dimensional numerical model analyses were carried out with $NT = 8192$, which renders a time interval $\Delta t = 0.2249$. The number of sampling points for the two-dimensional numerical models of the one-dimensional examples, indicated in the appropriate sections, is much smaller than $NT = 8192$ mentioned above. This excessively high NT value adopted aimed at leaving no doubt about the one-dimensional numerical model results accuracy. In fact one-dimensional numerical models results are so accurate that they were also used as analytical solution.

5.1 One-dimensional rod under sinusoidal initial displacement

The first example, shown in Fig. 1, consists of a one-dimensional rod under initial displacement with sinusoidal space dependence, as follows:

$$u(X, 0) = u_o(X) = A \sin\left(\frac{\pi x}{a}\right) \quad (21)$$

where A is the amplitude ($A = 1$ in this case). Fig. 2 shows the boundary mesh used for the two-dimensional analysis. The selected internal points at which the numerical responses were computed are on the horizontal line $y = 0$. The two-dimensional numerical model

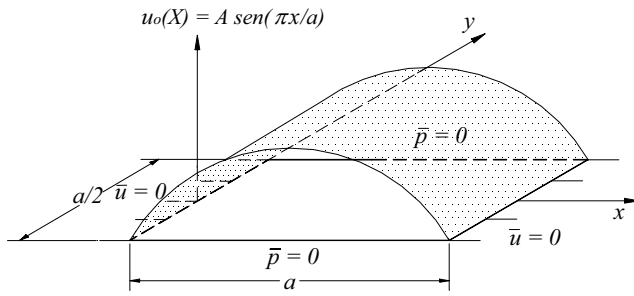


Figure 1 : One-dimensional rod under sinusoidal initial displacement: geometry, boundary and initial conditions.

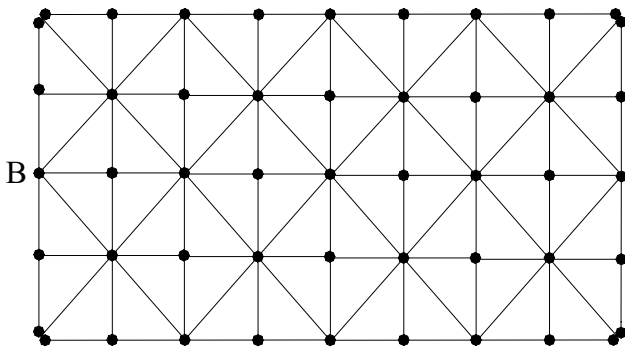


Figure 2 : One-dimensional rod under sinusoidal initial displacement: 2D boundary and domain discretization.

employed twenty four linear elements, resulting in $NN = 28$ boundary nodes, 64 linear cells for the entire domain discretization, $NT = 2048$, resulting in a time interval $\Delta t = 0.8996$, being the parameter $\beta = 0.60$. Eight linear one-dimensional cells were employed in the one-dimensional numerical analysis.

In Fig. 3 the responses due to the displacement sinusoidal initial condition are compared against the 1D responses.

5.2 Square membrane under prescribed discontinuous initial velocity

This example consists of a square membrane under prescribed initial velocity as shown in Fig. 4, i.e.:

$$v_o(X) = c; \quad \left(\frac{3a}{8} \leq x \leq \frac{5a}{8}, \frac{3a}{8} \leq y \leq \frac{5a}{8} \right) \quad (22)$$

whose boundary is fixed.

Fig. 5 shows the boundary mesh used with 64 boundary nodes and the internal point C selected. For this analysis

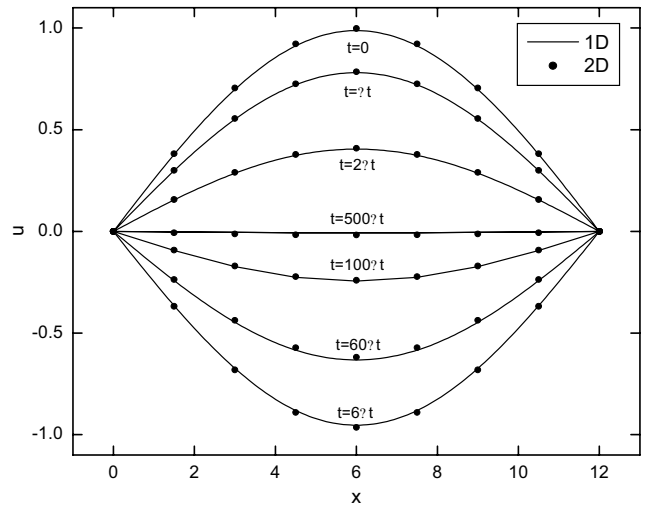


Figure 3 : Comparison of displacements for 1D and 2D numerical models for the one-dimensional rod under sinusoidal initial displacement.

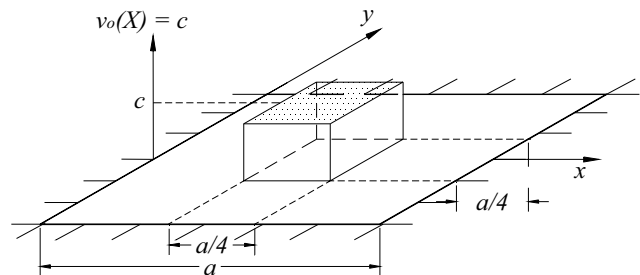


Figure 4 : Square membrane analysis: geometry and boundary conditions.

8 linear triangular cells were employed.

In Fig. 6 the response at point C for $\zeta = 0.25$, $\Delta t = 0.03$ and $NT = 4096$ are compared with the dampingless analytical response presented by Mansur (1983); here the extended period is $2Tp = 123$ and $\beta = 0.48$. Fig. 7 shows similar responses at point C for $\zeta = 0.025$, $\Delta t = 0.025$ and $NT = 8192$, the extended period is $2Tp = 205$ and $\beta = 0.4$.

5.3 One-dimensional rod under initial conditions prescribed over the entire domain

This example consists of a one-dimensional rod fixed at $x = a$, under a Heaviside-type forcing function applied at $x = 0$, at $t = 0$ and kept constant from this time

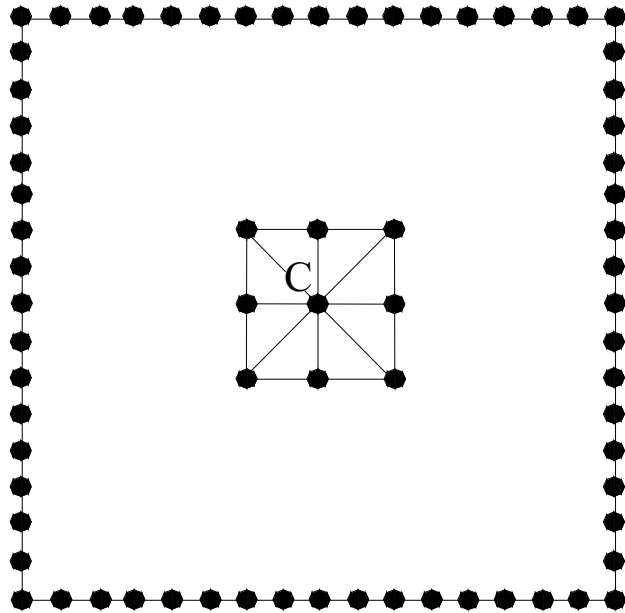


Figure 5 : Square membrane analysis: boundary and cell discretization and internal point C .

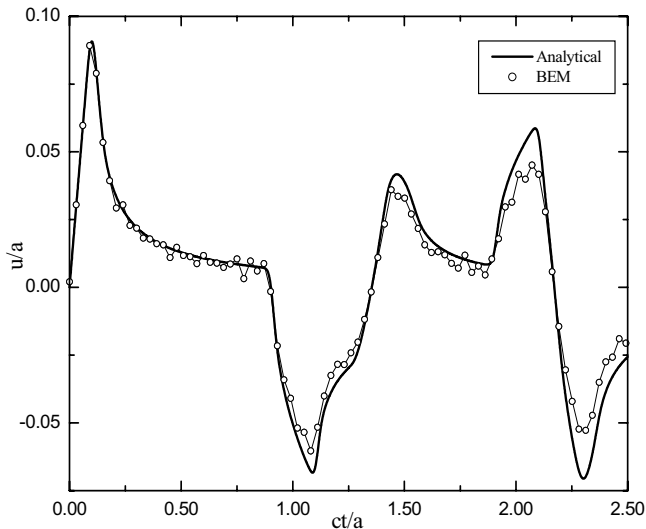


Figure 6 : Displacement time history for the membrane under prescribed initial velocity for $\zeta = 0.25$.

onwards, i.e., $\bar{p}(t) = P/E H(t - 0)$ as shown in Fig. 8. Initial displacements and velocities at $t = 0$, shown in

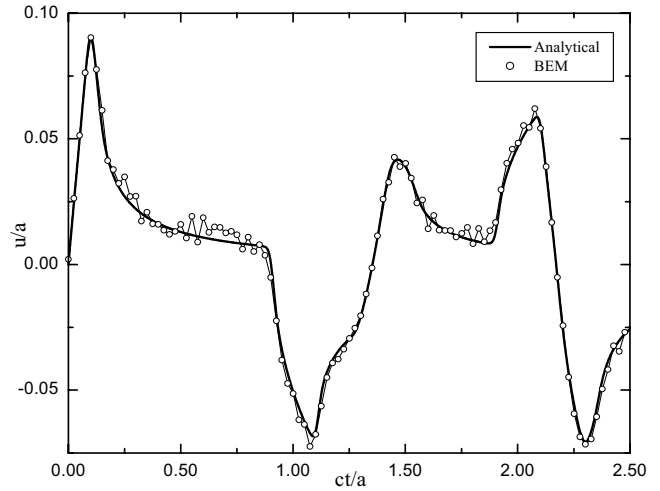


Figure 7 : Displacement time history for the membrane under prescribed initial velocity for $\zeta = 0.025$.

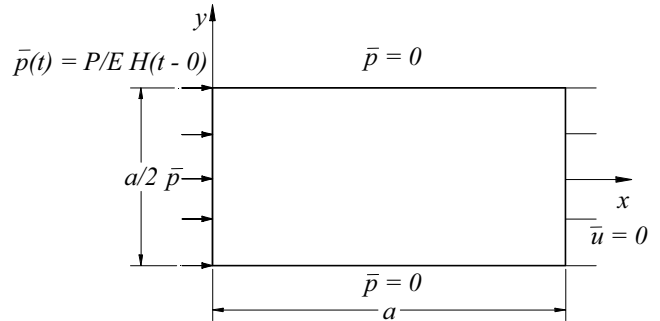


Figure 8 : One-dimensional rod under initial conditions prescribed over the entire domain: geometry and boundary conditions.

Fig. 9 and 10 respectively, are given by:

$$u_o(X) = \frac{P}{E} (a - x);$$

$$v_o(X) = \frac{Pc}{E} \left(0 \leq x \leq a, -\frac{a}{4} \leq y \leq \frac{a}{4} \right) \quad (23)$$

The mesh is the same already depicted in Fig. 2.

Fig. 11 depicts two curves which represent the time histories at point B represented in Fig. 2 due to the initial displacement and due to the initial velocity; whereas in Fig. 12 results considering all the contributions together are plotted. Fig. 12 also displays displacement time history due to the boundary load only ($u_o = v_o = 0$) which if shifted to the left by $t = a/c$ coincides with the re-

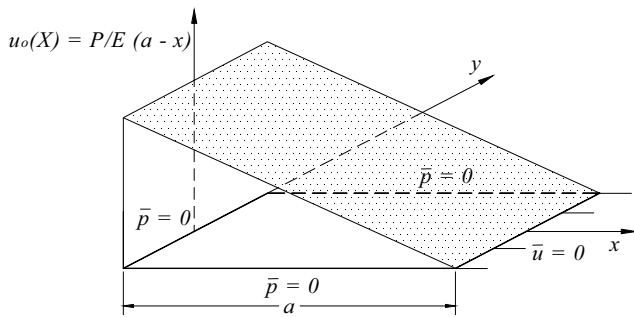


Figure 9 : One-dimensional rod under initial conditions prescribed over the entire domain: initial displacement.

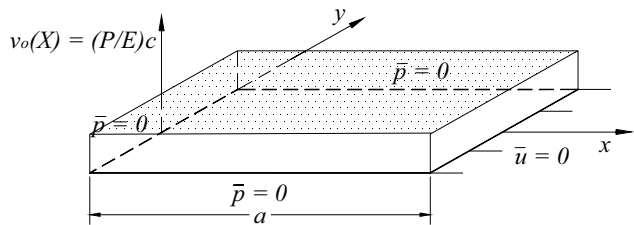


Figure 10 : One-dimensional rod under initial conditions prescribed over the entire domain: initial velocity.

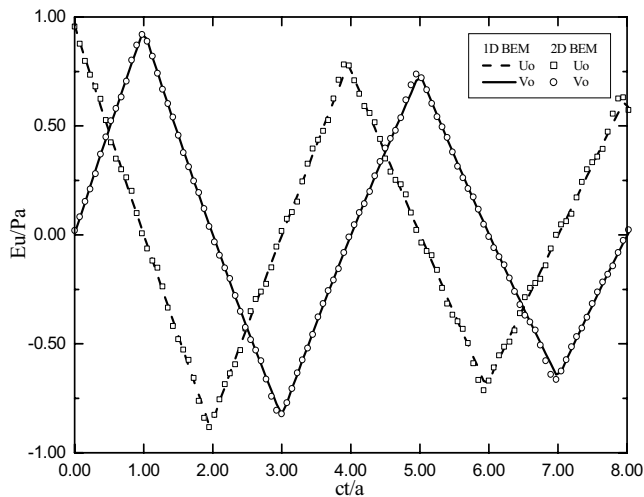


Figure 11 : One-dimensional rod under initial conditions prescribed over the entire domain: displacements for 1D and 2D numerical models for initial displacement and initial velocity plotted separately.

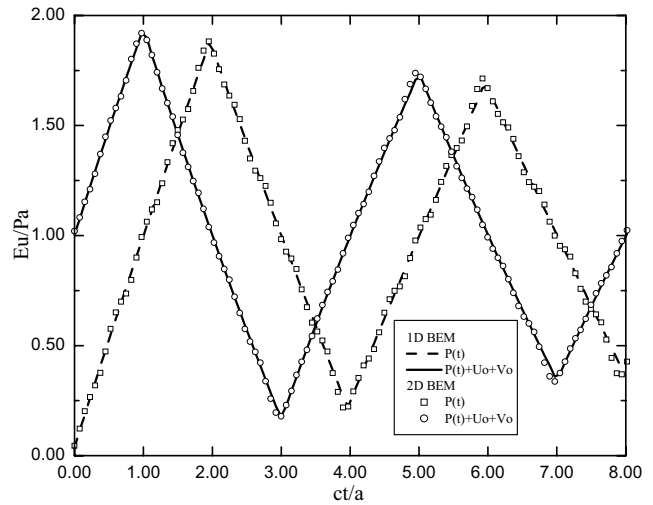


Figure 12 : Displacements at point D for the one-dimensional rod under initial conditions prescribed over the entire domain: effects of boundary load $p(t)$, initial displacement u_o and initial velocity v_o considered together. Also plotted the time-history due to $p(t)$ only.

sponse obtained considering initial conditions given by expression (23). In the present example all 2D analyses were carried out with $NT = 2048$ and $2Tp = 1842.0681$, the time interval is $\Delta t = 0.8994$ and $\beta = 0.60$.

It is important to notice that in the present example, x_{u_o} shown in expression (15) is due to two boundary loads (line loads) applied at $x = 0$ (boundary flux) and $x = a$.

5.4 One-dimensional rod under initial conditions prescribed over a subdomain

This example consists of a one-dimensional rod under a Heaviside-type forcing function applied in a similar way as that of the previous example, (see Fig. 8) subjected to initial displacements and velocities, shown in Fig. 13 and Fig. 14, respectively, given by:

$$u_o(X) = \frac{P}{E} \left(\frac{a}{4} - x \right);$$

$$v_o(X) = \frac{Pc}{E} \left(0 \leq x \leq \frac{a}{4}, -\frac{a}{4} \leq y \leq \frac{a}{4} \right) \quad (24)$$

Fig. 15 represents the boundary element mesh and the point D selected: in this analysis 48 boundary elements and 64 linear triangular cells were used. An important aspect concerning this example must be stated now: line forces appear where $grad(u_o(X))$ is discontinuous. In

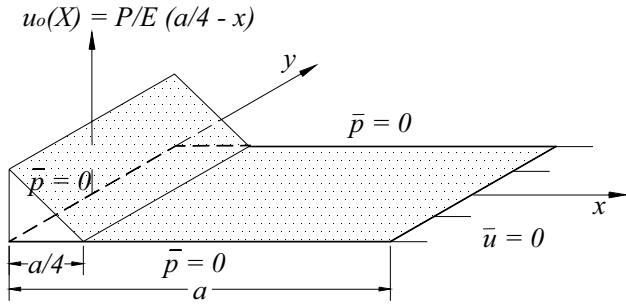


Figure 13 : One-dimensional rod under initial conditions prescribed over a subdomain: initial displacement.

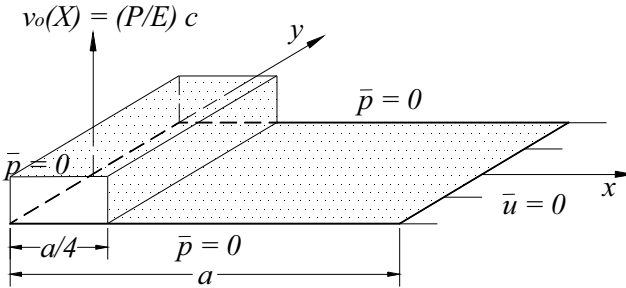


Figure 14 : One-dimensional rod under initial conditions prescribed over a subdomain: initial velocity.

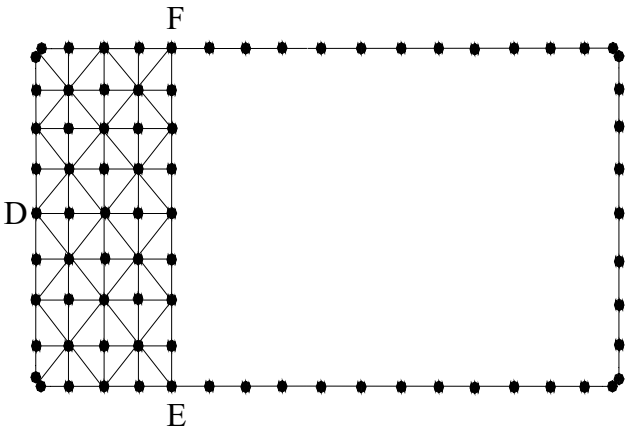


Figure 15 : One-dimensional rod under initial conditions prescribed over a subdomain: boundary discretization and cells.

this particular example, the volume integral that appears in the boundary integral equation (1) is reduced to line integrals. According to the previous observation, the

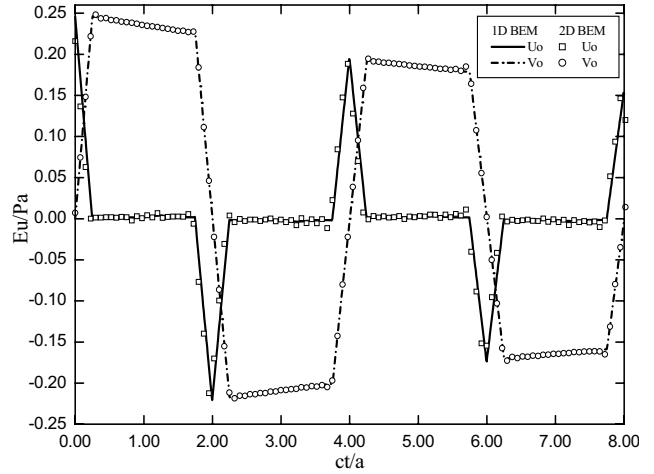


Figure 16 : One-dimensional rod under initial conditions prescribed over a subdomain: displacements for 1D and 2D numerical models for prescribed initial displacement and prescribed initial velocity plotted separately.

pseudo-forces which account for initial displacements contribution are constituted only by two line sources: one is a body force along the line $x = a/4$ and the other is a boundary flux along the boundary $x = 0$. Thus $B(X)$ in eq. (1) is equal to $-(P/E)\delta(x - a/4)$ and the volume integral indicated there becomes a line integral along the segment EF in Fig. 15:

$$-\int_E^F u^*(X, \xi)|_{x=a/4} d\Omega \quad (25)$$

Fig. 16 presents separate plots representing initial displacement and velocity contributions at point D only; and Fig. 17 depicts results in which the initial conditions are null ($u_o = v_o = 0$) and the total contribution where boundary conditions and initial conditions contributions are added together. Note that the corresponding 1D results are also presented, and that the curves representing the response due to the boundary load only and that which includes boundary load and initial conditions are shifted by a time equal to $a/4c$. The numerical parameters of this analyses were the same as those of the previous one except for the β parameter which was considered equal to 1.20 in the present case.

6 Remarks

The discussion presented in previous sections shows that the present formulation gives quite accurate results pro-

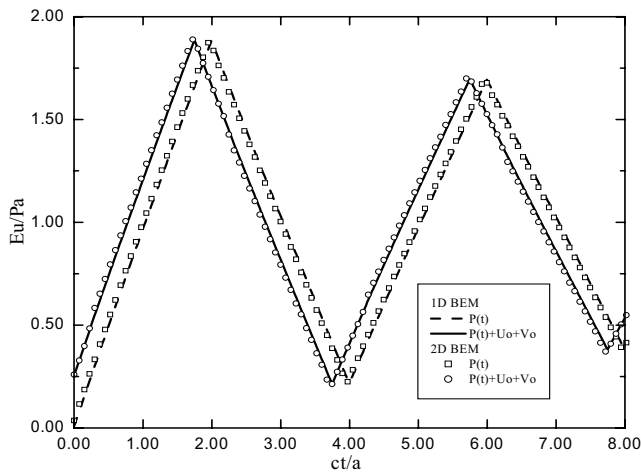


Figure 17 : Displacements at point D for the one-dimensional rod under initial conditions prescribed over a subdomain: effects of boundary load $p(t)$, initial displacement u_o and initial velocity v_o considered together. Also plotted the time-history due to $p(t)$ only.

vided good space and time discretization are employed. Time response curves presented separately show that time history due to either initial displacement or initial velocity are quite accurate. Total results shown, where boundary and initial conditions effects were considered together, were also very accurate, meaning that the superposition of these effects does not generate any significant time shifting or other disturbing effect. It is worth noting that Fig. 6 and Fig. 7 display a small amount of oscillation: expected, as the time-domain surface traction is singular for a discrete number of time instant; it is in fact difficult to obtain oscillation free results from IFFT (or IDFT) algorithms in this case. As expected, the oscillation level shown in Fig. 6 is lower than that shown in Fig. 7, as the damping concerning the former is higher than that of the latter.

7 Conclusions

The present work presents a BEM formulation which allows for the computation of initial conditions contribution in frequency-domain analyses of transient scalar wave propagation problems. In the approach described here, named ICPF (Initial Conditions by Pseudo-Forces) initial displacement and velocity are replaced by equivalent pseudo-forces represented with help of generalized functions. A number of examples was presented in order

to demonstrate the excellent accuracy of the results, and to illustrate the required time and space discretization refinement.

The approach presented here not only enhances the range of applications of BEM frequency-domain approaches, as non-null initial conditions contribution can now be considered, but can equally be followed when other numerical methods, e.g., Finite Elements, Finite Differences, Finite Volumes, etc., are employed, as the developments presented concern the differential equation itself, not the numerical algorithm. Thus, the present approach can also be used when transforms other than Fourier are employed (e.g., Laplace, Hankel, Wavelets, etc.).

Finally, it is important to highlight that the application presented here concerned 2D scalar wave propagation problems; however, the formulation presented applies to a large number of other 2D and 3D problems, e.g., acoustic, seismic and electromagnetic waves, dynamic analysis of structures, soil-fluid-structures interaction, etc.

References

- Antes, H.; Von Estorff, O.** (1987): On Causality in Dynamic Response Analysis by Time-dependent Boundary Element Methods. *Earthquake Engineering and Structural Dynamics*, vol. 15, pp. 865-870.
- Brighan, E. O.** (1974): *The Fast Fourier Transform*, Prentice-Hall, New Jersey.
- Carrer, J. A. M.; Mansur, W. J.** (1996): Time-domain BEM Analysis for the 2D Scalar Wave Equation: Initial Condition Contributions to Space and Time Derivatives. *International Journal for Numerical Methods in Engineering*, vol. 39, pp. 2169-2188.
- Carrer, J. A. M.; Telles, J. C. F.** (1992): A Boundary Element Formulation to Solve Transient Dynamic Elastoplastic Problems. *Computer and Structures*, vol. 45, pp. 707-713.
- Chin, W. C.** (1994): *Wave Propagation in Petroleum Engineering*, Gulf Publishing Company, Houston.
- Clough, R. W.; Penzien, J.** (1993): *Dynamics of Structures*. (2 ed) McGraw-Hill, New York.
- Cruse, T. A.; Rizzo, F. J.** (1968): A Direct Formulation and Numerical Solution of the General Transient Elastodynamic Problem I. *J. Math. Anal. Appl.*, vol. 22, pp. 244-259.

- Cruse, T. A.; Rizzo, F. J.** (1968): A Direct Formulation and Numerical Solution of the General Transient Elastodynamic Problem II. *J. Math. Anal. Appl.*, vol. 22, pp. 341-355.
- Dominguez, J.** (1993): *Boundary Elements in Dynamics*. Computational Mechanics Publications, Southampton and Boston.
- Dubner, H.; Abate, J.** (1983): Numerical Investigation of Laplace Transforms by Relating them to the Finite Fourier Cosine Transform. *Journal of the Association for Computing Machinery*, vol. 15, pp. 115-123.
- Durbin, F.** (1974): Numerical Inversion of Laplace Transforms: an Efficient Improvement to Dubner and Abate's Method. *Computer Journal*, vol. 17, pp. 371-376.
- Gaul, L.; Schanz, M.** (1999): A Comparative Study of Three Boundary Element Approaches to Calculate the Transient Response of Viscoelastic Solids with Unbounded Domains. *Computer Methods in Applied Mechanics and Engineering*, vol. 179, pp. 111-123.
- Gaul, L.; Wenzel, W.** (2002): A Coupled Symmetric BE-FE Method for Acoustic Fluid-structure Interaction. *Engineering Analysis with Boundary Elements*, vol. 26, pp. 629-636.
- Godinho, L.; Tadeu, A.; Branco, F. J.** (2003): Wave Scattering by Infinite Cylindrical Shell Structures Submerged in a Fluid Medium. *Wave Motion*, vol. 1134, pp. 1-19.
- Graff, K. F.** (1975): *Wave Motion in Elastic Solids*, Dover Publications, New York.
- Hatzigeorgiou, G. D.; Beskos, D. E.** (2001): Transient Dynamic Response of 3D Elastoplastic Structures by the D/BEM. In: D. E. Beskos; C. A. Brebbia; J. T. Katsikadelis; G. D. Manolis (ed) *Proceeding of Boundary Elements XXIII*. Lemnos, Greece.
- Lubich, C.** (1988): Convolution Quadrature and Discretized Operational Calculus I. *Numerische Mathematik*, v. 52, pp. 129-145.
- Lubich, C.** (1988): Convolution Quadrature and Discretized Operational Calculus II. *Numerische Mathematik*, v. 52, pp. 413-425.
- Manolis, G. D.; Beskos, D. E.** (1981): Dynamic Stress Concentration Studies by Boundary Integrals and Laplace Transform. *International Journal for Numerical Methods in Engineering*, vol. 17, pp. 573-599.
- Mansur, W. J.; Carrer, J. A. M.; Siqueira, E. F. N.** (1998): Time Discontinuous Linear Traction Approximation in Time Domain BEM Scalar Wave Propagation Analysis. *International Journal for Numerical Methods in Engineering*, vol. 42, pp. 667-683.
- Mansur, W. J.; DeLima-Silva, W.** (1992): Efficient Time Truncation in Two-Dimensional BEM Analysis of Transient Wave Propagation Problems. *Earthquake Engineering and Structural Dynamics*, vol. 21, pp. 51-63.
- Mansur, W. J.; Ferreira, W. G.; Claret, A. M.; Venâncio-Filho, F.; Carrer, J. A. M.** (2000): Time-Segmented Frequency-Domain Analysis for Non-Linear Multi-Degree-of-Freedom Structural Systems. *Journal of Sound and Vibration*, vol. 237, pp. 458-475.
- Mansur, W. J.; Abreu, A. I.; Carrer, J. A. M.; Ferro, M. A. C.** (2002): Wave Propagation Analysis in The frequency Domain: Initial Conditions Contribution. In: C. A. Brebbia; A. Tadeu; V. Popov (ed) *Proceeding of Boundary Elements XXIV*, Sintra, Portugal.
- Mansur, W. J.** (1983): A Time-Stepping Technique to Solve Wave Propagation Problems Using the Boundary Element Method. *Ph.D. Thesis*, University of Southampton, England.
- Morse, P. M.; Feshbach, H.** (1953): *Methods of Theoretical Physics*, McGraw-Hill, New York.
- Nardini, D.; Brebbia, C. A.** (1985): Applications of an Alternative Boundary Element Procedure in Elastodynamics, In: *Topics in Boundary Element Research*, vol. 2: Southampton and Springer-Verlag, Berlin and New York.
- Oppenheim, A. V.; Schafer, R. W.** (1989): *Discrete Time Signal Processing*, Prentice Hall Englewood Cliffs, New Jersey.
- Partridge, P. W.; Brebbia, C. A.; Wrobel, L. C.** (1992): The Dual Reciprocity Boundary Element Method. *Computational Mechanics Publications, Southampton Boston and New York*.
- Paz, M.** (1997): *Structural Dynamics—Theory and Computation*, (4 ed) Chapman and Hall, New York.
- Sellountos, E. J.; Polyzos, D.** (2003): A MLPG (LBIE) Method for Solving Frequency Domain Elastic Problems. *CMES: Computer Modeling in Engineering & Sciences*, vol. 4, no. 6, pp. 619-636.
- Veletsos, A.; Ventura, C.** (1984): Efficient Analysis of Dynamic Response of Linear Systems. *Earthquake En-*

gineering and Structural Dynamics, vol. 12, pp. 521-536.

Veletsos, A.; Ventura, C. (1985): Dynamic Analysis of Structures by the DFT Method. *Journal of Structural Engineering ASCE*, vol. 111, pp. 2625-2642.

Zhang, Ch.; Savaidis, A. (2003): 3-D Transient Dynamic Crack Analysis by a Novel Time-Domain BEM. *CMES: Computer Modeling in Engineering & Sciences*, vol. 4, no. 5, pp. 603-618.